



Low-cost silica based ceramic supported thin film composite hollow fiber membrane from guinea corn husk ash for efficient removal of microplastic from aqueous solution

Lukka Thuyavan Yogarathinam^a, Jamilu Usman^{a,b}, Mohd Hafiz Dzarfan Othman^a, Ahmad Fauzi Ismail^{a,*}, Pei Sean Goh^a, Arthanareeswaran Gangasalam^c, Mohd Ridhwan Adam^a

^a Advanced Membrane Technology Research Centre (AMTEC), School of Chemical and Energy Engineering, Universiti Teknologi Malaysia, 81310, Skudai, Johor, Malaysia

^b Department of Chemistry, Faculty of Science, Sokoto State University, P.M.B. 2134, Sokoto, Sokoto State, Nigeria

^c Membrane Research Laboratory, Department of Chemical Engineering, National Institute of Technology Tiruchirappalli, 620015, India

ARTICLE INFO

Editor: Lingxin Chen

Keywords:

Ceramics

Fouling

Thin film composite

Hollow fiber membrane

Microplastics

ABSTRACT

In this study, an economic silica based ceramic hollow fiber (HF) microporous membrane was fabricated from guinea cornhusk ash (GCHA). A silica interlayer was coated to form a defect free silica membrane which serves as a support for the formation of thin film composite (TFC) ceramic hollow fiber (HF) membrane for the removal of microplastics (MPs) from aqueous solutions. Polyacrylonitrile (PAN), polyvinyl-chloride (PVC), polyvinylpyrrolidone (PVP) and polymethyl methacrylate (PMMA) are the selected MPs. The effects of amine monomer concentration (0.5 wt% and 1 wt%) on the formation of poly (piperazine-amide) layer via interfacial polymerization over the GCHA ceramic support were also investigated. The morphology analysis of TFC GCHA HF membranes revealed the formation of a poly (piperazine-amide) layer with narrow pore arrangement. The pore size of TFC GCHA membrane declined with the formation of poly (piperazine-amide) layer, as evidenced from porosimetry analysis. The increase of amine concentration reduced the porosity and water flux of TFC GCHA HF membranes. During MPs filtration, 1 wt% (piperazine) based TFC GCHA membrane showed a lower transmission percentage of PVP (2.7%) and other suspended MPs also displayed lower transmission. The impact of humic acid and sodium alginate on MPs filtration and seawater pretreatment were also analyzed.

1. Introduction

Plastics are polymer-based materials with unique characteristics such as highly durable, high electrical and thermal insulation, high chemical stability, low cost, and can be easily mass-produced. Due to their various properties, they have been extensively utilized in a variety of industries, including packaging, manufacturing, textiles, electronic devices and home appliances, and machinery. With a large production volume, most plastic-related trash ends up in the environment as a result of human negligence (Wang et al., 2020a). Microplastics (MPs) are an emerging persistent freshwater and ocean pollutant with particle size less than 5 mm. Polystyrene (PS), polypropylene (PP), polyvinyl-chloride (PVC), polyethylene (PE), polycarbonate (PC), polyamides (PA) polyester (PES), and polyethylene terephthalate (PET) are examples of prevalent MPs found in seawater and wastewater treatment

plant (Kumar et al., 2021a, 2021b). MPs have disastrous eco-toxicological impact on marine species and human beings (Kumar et al., 2021a, 2021b; Sun et al., 2019). It causes the (i) damage of human cells and inflammation, (ii) toxic effect by diffusion of secondary plastic products upon degradation and (iii) toxic ingestion by marine micro-organism (Bilal and Iqbal, 2020; Dick Vethaak and Legler, 2021). Therefore, it is mandatory to eliminate MPs from aqueous environment.

Polymeric microfiltration and ultrafiltration membranes have been primarily employed to remove polyamide, poly(ethylene) and polystyrene (Enfrin et al., 2020; Pizzichetti et al., 2021). However, flux decline and membrane fouling have hampered their applications for MPs filtration. The tendency of membrane fouling by MP is affected by the size, shape and physiochemical properties (hydrophobic/hydrophilic and charge). Organic fouling phenomenon occurs with an initial adsorption of MPs on the membrane pores which results

* Corresponding author.

E-mail address: afauzi@utm.my (A.F. Ismail).

<https://doi.org/10.1016/j.jhazmat.2021.127298>

Received 28 May 2021; Received in revised form 1 September 2021; Accepted 17 September 2021

Available online 20 September 2021

0304-3894/© 2021 Elsevier B.V. All rights reserved.

in the formation of either reversible or irreversible cake layer (Enfrin et al., 2021). Polymeric membranes are deployed widely for industrial wastewater treatment but it is sensitive to chemical reaction that greatly affects its performance and life span (Fard et al., 2018). To circumvent the effect, ceramic MF and UF membranes have been used for the reclamation of industrial wastewater as they exhibit good chemical and thermal stability, extended life span and can be cleaned with simpler protocols. Expensive materials like titania, zirconia and alumina have been used as raw materials for the fabrication of ceramic supports (Khanmohammadi et al., 2020; Van Gestel et al., 2006). Over time, researchers explored different low-cost alternatives like sugarcane bagasse and rice husk ash to produce environmentally-benign silica based ceramic membrane for water treatment (Hubadillah et al., 2017; Jamalludin et al., 2019). The common sources of raw materials used in the fabrication of low-cost ceramic membrane for wastewater applications are tabulated in Table 1. Agro-based ash is a preferable source for the fabrication of ceramic membranes as it is silica-rich and abundantly available. The main advantages of utilizing biomass based materials for ceramic membrane fabrication are related to the (i) cost-effectiveness, (ii) ability to form defect-free resilient asymmetric porous membrane with multifunctions (selective adsorption, catalytic & sieving) due to presence of silica metal oxides with other constituents (carbon and other metal oxides) and (iii) ease of functionalization (Hubadillah et al., 2020, 2018, 2017). Guinea corn (*Sorghum vulgare*) husk (GCH) is an abundant and cheap source of silica (94% of silica) that has been used as a raw material for cement additives, adhesives and polymer. (Bello et al., 2018). In this study, a novel ceramic thin film composite (TFC) hollow fiber HF membrane supported by guinea cornhusk ash (GCHA) has been fabricated for the treatment of MPs containing wastewater. The chosen model MPs are polyacrylonitrile (PAN), polyvinyl-chloride (PVC), polyvinylpyrrolidone (PVP) and polymethyl methacrylate (PMMA). These MPs have been widely used as binders and precursors in various industrial applications and their molecular weight are in the range of few hundred kilodaltons (kDa).

Ceramic substrates are very porous hence highly susceptible to pore blocking during the filtration of suspended and large sized MPs. To control fouling and improve the membrane's rejection, TFC membranes, with a polyamide selective layer formed atop of the highly porous substrate, have been developed in recent years (Gohil and Ray, 2017). Recently, ceramic supported TFC membranes have been investigated for pervaporation (Zhang et al., 2021a) and dye filtration (Xia et al., 2018) applications. Literature indicates that the monomer concentration and intermediate layer have significant influence towards the polyamide layer formation and the mechanisms involved in the pollutant removal. Studies on the fabrication of ceramic membrane-based GCHA have not yet been reported. The literatures on MPs filtration are also sparsely reported. Therefore, this study aims to provide further understanding on the construction of an antifouling ceramic supported TFC membrane for

effective MPs separation. The study constitutes of: (i) the fabrication and characterization of GCHA HF membrane and formation of polyamide layer over TFC membrane via interfacial polymerization. The intermediate silica layer was prepared as a compatible substrate to form a defect free polyamide layer. The influence of two different concentrations of amine monomers was also studied. (ii) comparison of the filtration performance of GCHA HF and TFC GCHA HF for MPs filtration in aqueous solution. The impact of organic foulants (humic acid (HA) and sodium alginate (SA) on MPs filtration was evaluated. The feasibility and long-term stability of TFC GCHA HF membranes for seawater pre-treatment were also studied.

2. Experimental

2.1. Materials

Polyethersulfone (PES) was purchased from Solvay and used as polymer binder in GCHA dope solution preparation. N-Methyl-2-Pyrrolidone (NMP) was used as solvent, which was procured from Merck. Arlacel P135 gel was obtained from CRODA. Absolute ethanol and ammonia were used for silica sol preparation, which was obtained from Merck. Tetraethyl-orthosilicate (TEOS) (98%) was procured from Sigma and was used as precursor material for the silica. The chosen model microplastic such as polyvinylpyrrolidone (PVP 360,000) polyacrylonitrile (PAN), polyvinyl-chloride (PVC), and polymethyl methacrylate (PMMA 120,000) were purchased from Merck.

2.2. Fabrication of GCHA and TFC-GCHA hollow fiber (HF) membrane

2.2.1. Fabrication of GCHA hollow fiber membrane

GCH was ground evenly and pyrolyzed at 800°C for 2 h with a heating rate of 5°C/min. Then, the GCH ash (GCHA) was mechanically sieved with mesh size of 20 µm. The silica composition of the sieved GCHA was revealed to be 71.1 wt% as determined through X-ray fluorescence (XRF) analysis. 35 wt% of 20 µm GCHA was used as the base material for the fabrication of HF ceramic membrane through a dual orifice spinneret via phase inversion and sintering method. Firstly, 1 g of arcel was dissolved in 59 g of NMP under constant stirring for 2 h. Then, 35 g of dried GCHA powder was added into the NMP solution ball milled for 48 h. Next, 5 g of binder (PES) was added into the ceramic suspension and again ball milled for another 48 h. Prior to spinning, the dope solution was degassed under vacuum condition for 30 min. Then, the bubble free dope solution was poured into a stainless-steel syringe. The ceramic hollow fiber support membrane was extruded at a rate of 10 ml/min through a spinneret and into a custom designed hollow fiber spinning system, using water as non-solvent of choice. Reverse osmosis water, which was used as a bore fluid, was extruded at a rate of 9 ml/min. The outer and inner diameters of the spinneret were fixed at 2.8 and 0.5 mm, respectively. The collected ceramic GCHA HF was immersed in a water bath for 24 h and dried at room temperature for 48 h. Finally, the GCHA HF membranes were sintered at 1100°C for 5 h.

2.2.2. Fabrication of TFC- GCH hollow fiber membrane

Silica sol coating was employed to provide a hydrophilic layer for the formation of poly (piperazine-amide) layer (Usman et al., 2020). Prior to TFC formation, GCHA membrane was hydrolyzed by immersing in an ethanol:water (50:50) mixture for 24 h. Then, the hydrolyzed GCHA HF membrane was immersed in a silica sol solution for 1 h and followed by drying in a vacuum oven at 100°C for 1 h. Three cycles of silica sol coating were carried out and calcined at 400°C for 2 h. Then, the GCHA sol coated HF membrane was subjected to TFC membrane fabrication. Preparation of silica sol solution followed the Stober method the synthesis of silica sol and TEOS was used as the silica precursor material. 0.24 M TEOS was initially dissolved in a 4.64 M ethanol solution. Then, the precursor solution was slowly dropped into the reaction mixture containing 1.04 M ammonia, 4.0 M water and 4.64 M ethanol solution

Table 1
Cost-effective raw material based ceramic membrane for wastewater treatment application.

Ceramic membranes	sources	Mechanism	Application	References
Aluminosilicate	kaolin	sieving	oily wastewater	(Vinoth Kumar et al., 2015)
Hydroxyapatite	cow bone	sieving	textile wastewater	(Hubadillah et al., 2020)
Aluminosilicate	natural zeolite	adsorption	ammonia wastewater	(Adam et al., 2019)
Silica	Natural clay	sieving	synthetic dyes wastewater	(Ouaddari et al., 2019)
Silica	silica sand	sieving	oily wastewater	(Alftessi et al., 2021)
Aluminosilicate	fly ash and kaolin	sieving	oily wastewater	(Zou et al., 2021)

using a dropper. The colloidal silica sol was allowed to form at 60°C for 90 min and aged for 3 days. Then, the GCHA HF membrane was sealed at both ends using epoxy resin.

2.2.3. Fabrication of TFC membrane

Interfacial polymerization method was adopted for the formation of poly (piperazine-amide layer) over GCHA HF membrane and the reaction between the monomers is schematically illustrated in Fig. 1. GCHA HF membrane was immersed in an aqueous amine monomer solution (piperazine and triethylamine (1 wt%) in water) for 8 min. Two different concentrations of piperazine 0.5 wt% and 1.0 wt% were used to study the influence of formation of poly (piperazine-amide) layer. Then, the GCHA HF membranes prepared at different monomer concentration were dried separately in atmospheric condition, followed by the immersion into acyl chloride monomer solution for 2 min (0.2 wt% of trimesoyl chloride (TMC) in hexane). The membranes were then dried in a vacuum oven at 60°C for 6 min. Two different monomer concentration based TFC membranes were stored in water and labeled as TFC GCHA-1 and TFC GCHA-2. The influence of piperazine on polyamide layer formation was studied by varying the concentration from 0.5 wt% to 1 wt% and the corresponding membranes were labeled as TFC-GCHA-1 HF and TFC-GCHA-2 HF, respectively.

2.3. Physicochemical characterization

The morphology and topography of GCHHF membrane were analyzed using scanning electron microscopy (SEM) (TM 3000, Hitachi) and atomic force microscopy (AFM) (5000II, Hitachi), respectively. The porosity of GCHA HF membranes were determined using mercury intrusion porosimetry (MIP) (MicroActive AutoPore V9600 Version 1.03).

2.4. Filtration performance analysis of GCAHF and TFC GCHA membranes

The MPs filtration experiments were conducted using a customized hollow fiber filtration module. The water flux was calculated based on the flowrate of feed solution (F (L/h)) and membrane surface (A) (m^2), using the Eq. (1).

$$J_w = \left(\frac{F}{A} \right) \quad (1)$$

Membrane permeability was obtained from the slope of plot between the flux and corresponding transmembrane pressure (TMP).

PVC, PAN and PMMA feed suspension were prepared by dispersion in reverse osmosis (RO) water using an ultrasonicator, whereas PVP was dissolved in RO water. Prior to MPs filtration, membranes were compacted at a TMP of 200 kPa until it attained a steady state flux. Then, each MPs solution was fed separately into the filtration cell and the flux corresponding to different TMP and concentration was monitored. The TMP was in the range of 50–200 kPa whereas the MPs concentrations were fixed at 50 mg/L and 100 mg/L. Membrane fouling was investigated using 50 mg/L of HA and SA as model foulants. The concentration of MPs was determined using a total organic carbon analyzer (Shimadzu TOC-L Total Organic Carbon Analyzer).

The concentration polarization model was used to understand the

transport mechanism of MPs in porous GCAHF and TFC GCHA membranes. Concentration polarization is a phenomenon of solute particle buildup on the membrane surface, which is also referred to as irreversible fouling. This occurs constantly when the solute size is bigger than the membrane's pore size. The generalized expression of volumetric flux (J_v) (m/s) relating to concentration gradient is expressed as follows (Lohokare et al., 2008).

$$J_v = k \ln \left(\frac{C_m - C_p}{C_b - C_p} \right) \quad (2)$$

where k is the mass transfer coefficient (m/s), C_m is the solute concentration on the surface of membrane, C_p and C_b are the permeate concentration and bulk concentration, respectively. In concentration polarization, the transmission of solute across the membrane is controlled by the boundary condition of C_m and C_b . To determine the mass transfer coefficient, transmission (τ) is introduced to Eq. (3) and arranged as

$$\ln \left(\frac{\tau_{obs}}{1 - \tau_{obs}} \right) = \ln \left(\frac{\tau}{1 - \tau} \right) + \frac{J_v}{k} \quad (3)$$

where τ_{obs} and τ are the observed transmission and true transmission, respectively. τ is the ratio of concentration of solute in permeate to concentration of solute at membrane surface. τ_{obs} is the observed transmission which is the ratio of concentration of solute in permeate to concentration of solute in bulk. The mass transfer coefficient was obtained from the slope of plot between J_v and $\ln \left(\frac{\tau_{obs}}{1 - \tau_{obs}} \right)$.

The long term pretreatment efficiency of the porous membrane was also evaluated using untreated seawater. The seawater samples were collected from Pantai Senok, Malaysia and the seawater characteristics was reported in our earlier studies (Lukka Thuyavan et al., 2021). The untreated seawater was filtered using a cross-flow HF module at the low TMP of 100 kPa for 120 min followed by washing with 0.2% sodium hydroxide solution and water. The saline solution was passed through the filtration cell again for another 120 min and the permeate was collected at the interval of 15 min. Flux reduction ratio (FRR) was calculated for the experiment of MPs filtration and seawater pretreatment using initial water flux (J_{iw}) and after water flux (J_{aw}), by Eq. (4).

$$\% \text{Flux reduction ratio (FRR)} = \left(\frac{J_{iw} - J_{aw}}{J_{iw}} \right) \times 100 \quad (4)$$

Fourier transform infrared (FTIR) spectroscopy (Thermo Scientific iS20 FT-IR spectrometer) was used to study the functional groups of membrane before and after filtration. Prior to FTIR analysis, the ceramic membrane was ground into a powder and formed into a pellet shape with potassium bromide (KBr).

3. Results and discussion

3.1. Surface and cross-sectional morphology analysis of GCHA and TFC-GCHA membranes

Fig. 2 shows the cross-sectional and surface morphological images of GCHA, TFC-GCHA-1 and TFC-GCHA-2 HF membranes. Referring to Fig. 2, typical asymmetric structures were noticed in GCHA, TFC-GCHA-

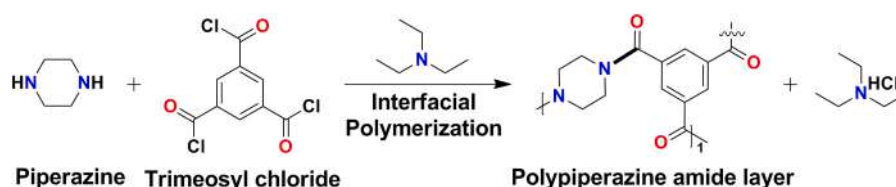


Fig. 1. Schematic illustration of polypiperazine-amide layer formation.

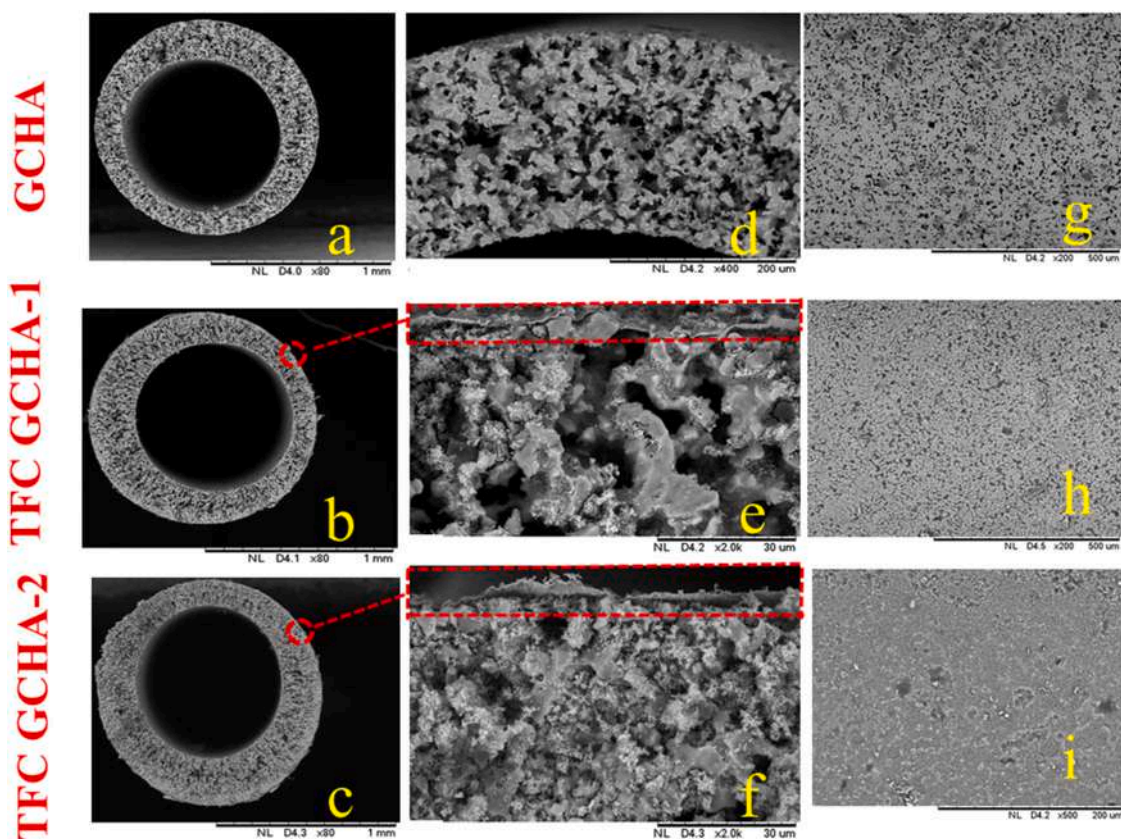


Fig. 2. Cross sectional (a-f) and surface (g-i) morphology analysis of GCHA, TFC-GCHA-1 and TFC-GCHA-2 HF membranes.

1 and TFC-GCHA-2 HF membranes. The GCHA support layer exhibited spongy and porous support layer formation with macrovoid formation. During phase inversion, GCHA powder with PES binder formed an asymmetric structure through the exchange between solvent and non-solvent in the coagulant bath (Yu et al., 2020). During GCHA sintering, PES was incinerated to form a porous substrate layer. Interestingly, thin poly (piperazine-amide) layer was clearly seen in both TFC-GCHA-1 and TFC-GCHA-2 HF membranes (Figs. 2e and 2f). Interlayer silica also enhanced the degree of densification in the macrovoid pores. It was observed that the increase in piperazine concentration from 0.5 to 1 wt % enhanced the monomer diffusion in the silica layer of HF membranes, hence resulting in an increase of skin layer. The thickness of poly (piperazine-amide) layer of TFC-GCHA-1 and TFC-GCHA-2 HF membranes are 280 and 332 nm, respectively. The dense layer ensures that the intermediate silica layer is rich with hydroxyl ions, providing a good

platform for the formation of poly (piperazine-amide) layer. As seen in Fig. 2g, large pores were clearly observed in GCHA HF membranes. The pore size reduced in both TFC-GCHA HF membranes, which was due to the interfacial polymerization between piperazine and TMC. Uniform and dense pores with continuous layer were noticed in TFC-GCHA-2 HF membrane, owing to higher degree of crosslinking between the monomers (Wei et al., 2011). Morphological analysis indicated that GCHA has good compatibility due to the formation of an asymmetric structure and poly (piperazine-amide) layer over the substrate.

3.2. AFM topography analysis of GCHA and TFC-GCHA membranes

Fig. 3 shows the AFM topography of GCHA and TFC-GCHA HF membranes. GCHA membrane displayed a wide peak-valley formation and high surface roughness of 220.5 nm (Fig. 3a), due to the large pore

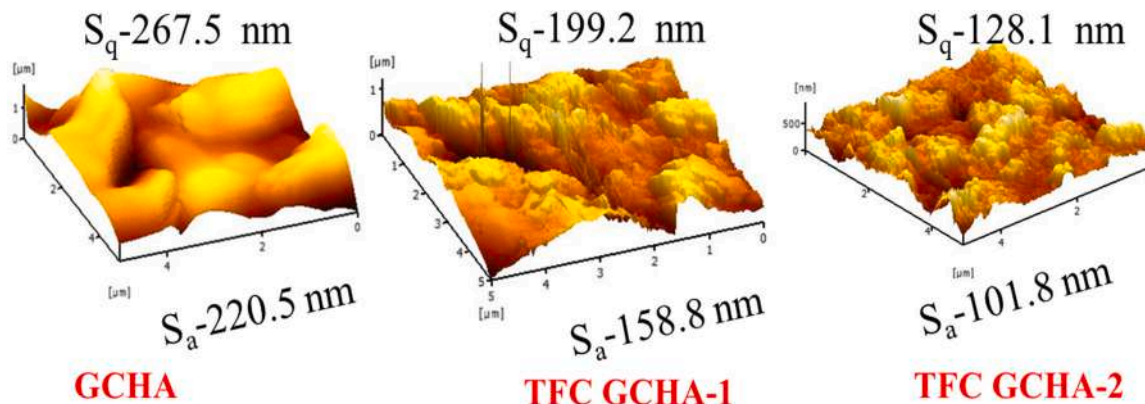


Fig. 3. AFM topography analysis of (a) GCHA, (b) TFC-GCHA-1 and (c) TFC-GCHA-2 HF membranes.

size. The high surface roughness was attributed to the quick exchange between solvent and non-solvent during phase separation. Furthermore, the GCHA also exhibited water retention properties, which led to instantaneous demixing and the formation of irregular and rougher surface. The poly (piperazine-amide) layer of TFC membrane exhibited lower peak-valley formation as a result of a regular pore development. The surface roughness decreased to 158.8 nm and 101.8 nm for TFC-GCHA-1 and TFC-GCHA-2 HF membranes, respectively (Figs. 3b and 3c). The pore size distribution was uniform in TFC-GCHA-2 HF membranes, due to the controlled diffusion of aqueous amine monomer (piperazine) to TMC region of reaction zone upon interfacial polymerization. In case of TFC-GCHA-1 membrane, lower concentration of piperazine altered the diffusion rate in polymerization zone and resulted in the increase in the number of unreacted TMC groups. Hence, the ridge-valley formation with higher surface roughness was observed. Similar pattern are observed with the literature of TFC polymeric RO membranes (Khorshidi et al., 2015; Yan et al., 2015). This clearly indicated that the polyamide layer constrained the pore formation on GCHA membrane. In general, membranes with lower surface roughness are less susceptible to adsorption of solutes upon filtration (Zhong et al., 2012). The as-fabricated TFC-GCHA may aid in restriction of MPs adsorption over the surface upon filtration.

3.3. Porosity analysis of GCHA and TFC-GCHA membranes

Fig. 4 shows the porosity analysis of GCHA, TFC-GCHA-1 and TFC-GCHA-2 HF membranes. As seen in Fig. 4, GCHA HF membrane displayed higher peak intensity and exhibited higher porosity of 76.03%, while this decreased to 44.89% for TFC-GCHA-2 HF membranes. The enhanced porosity of GCHA membrane was due to the selection of lower concentration of GCHA powder (35 wt%) and sintering temperature (1100°C). The larger pore sized membrane facilitated quick transport of water molecules across the channels, which enables filtration under lower TMP. The reduced porosity in TFC-GCHA membranes was due to the dense packing of macrovoid pores by silica interlayer and formation of outer polyamide layer. During interfacial polymerization (Fig. 1), amine monomer film diffuses towards the interface of organic TMC layer, which determine the thickness and porosity of the selective layer. The entire interfacial polymerization reaction is governed by the monomer concentration, reaction time temperature and type of monomer (Seah et al., 2020). It is imperative to note that the TFC-GCHA membranes possessed a smaller pore ranges from 0.11 to 0.18 μm as compared to GCHA HF, which owed to the formation of poly

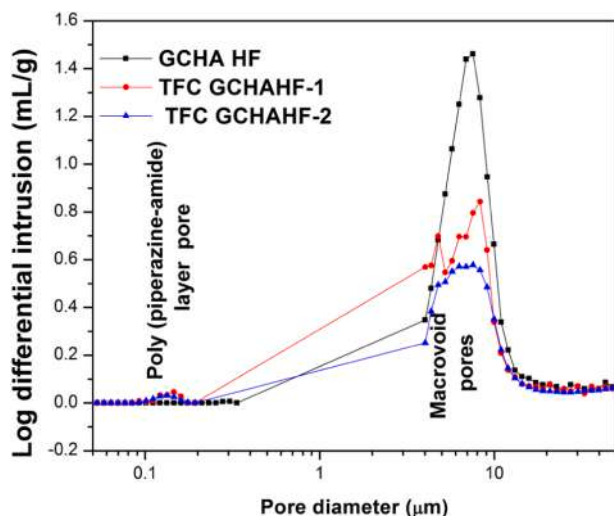


Fig. 4. Pore size and water flux analysis of GCHA, TFC-GCHA-1 and TFC-GCHA-2 membranes.

(piperazine-amide) layer (Fig. 4). It confirms that the thin polyamide layer was bound to the ceramic substrate. It also indicates that the pore size of GCHA HF membrane is similar to commercial high molecular weight cut off microfiltration (MF) membranes. As seen in Fig. 4, the intensity of poly (piperazine-amide) pore was slightly lower in TFC-GCHA-2 membranes. This phenomenon was due to the formation of pores with dense surface through the higher concentration of PIP. It enable the active sites of amine layer to form dense cross-linked poly (piperazine-amide) layer by the controlled diffusion of PIP to organic interface through acid acceptor triethylamine. Similar pore size reduction trend were also noticed in literature of TFC ceramic membrane (Chong and Wang, 2019). The pore size range indicated that the smaller pore size TFC-GCHA membrane can restrict the transport of micron range particles.

3.4. Water permeability analysis of GCHA and TFC-GCHA membranes

Fig. 5 shows the water permeability analysis of GCHA and TFC-GCHA membranes. GCHA membrane exhibited the highest water permeability of 4.27×10^{-5} m/s kPa. However, the water permeability decreased to 4.35×10^{-6} m/s kPa and 2.54×10^{-6} m/s kPa for TFC-GCHA-1 and TFC-GCHA-2 HF membranes, respectively. The higher water permeability value of GCHA membrane was due to the porous structure and the presence of abundant silica functional group. Silica constitutes of hydroxyl groups to enables fast absorption of water molecules upon phase separation. It eventually aids in the formation of porous structures. Thus, higher water flux of 6128.74 L/m²h was noticed at 200 kPa in GCHA membrane. From Fig. 5, the water flux TFC-GCHA membranes dropped significantly. It clearly depicted that the existence of poly (piperazine-amide) layer on ceramic substrate controlled the pore size formation. Compared to TFC-GCHA-1 membranes, TFC-GCHA-2 achieved a lower flux of 296.58 L/m²h due to forming of dense layer when higher concentration of piperazine cross linked with TMC.

3.5. MPs filtration performance analysis

3.5.1. Impact of TMP and concentration on MPs filtration analysis of GCHA and TFC-GCHA membranes

Fig. 6. shows the volumetric flux (J_v) versus transmission (τ) plots of MPs filtration (PVC, PMMA, PAN and PVP), as a function of TMP (50–200 kPa) and concentration (50 mg/L and 100 mg/L). As seen in Fig. 6, J_v increased with the increase of TMP, from 50–200 kPa. Among the membranes, GCHA membrane exhibited the highest J_v of 3.06×10^{-3} m/s at 200 kPa for 50 mg /L PVC suspension. The

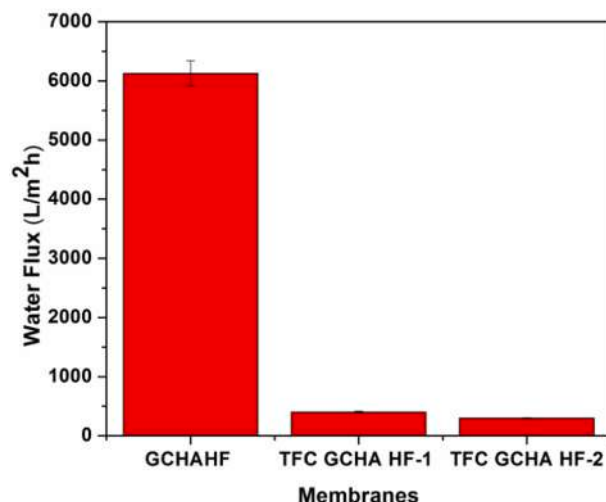


Fig. 5. Water flux analysis of GCHA and TFC-GCHA membranes.

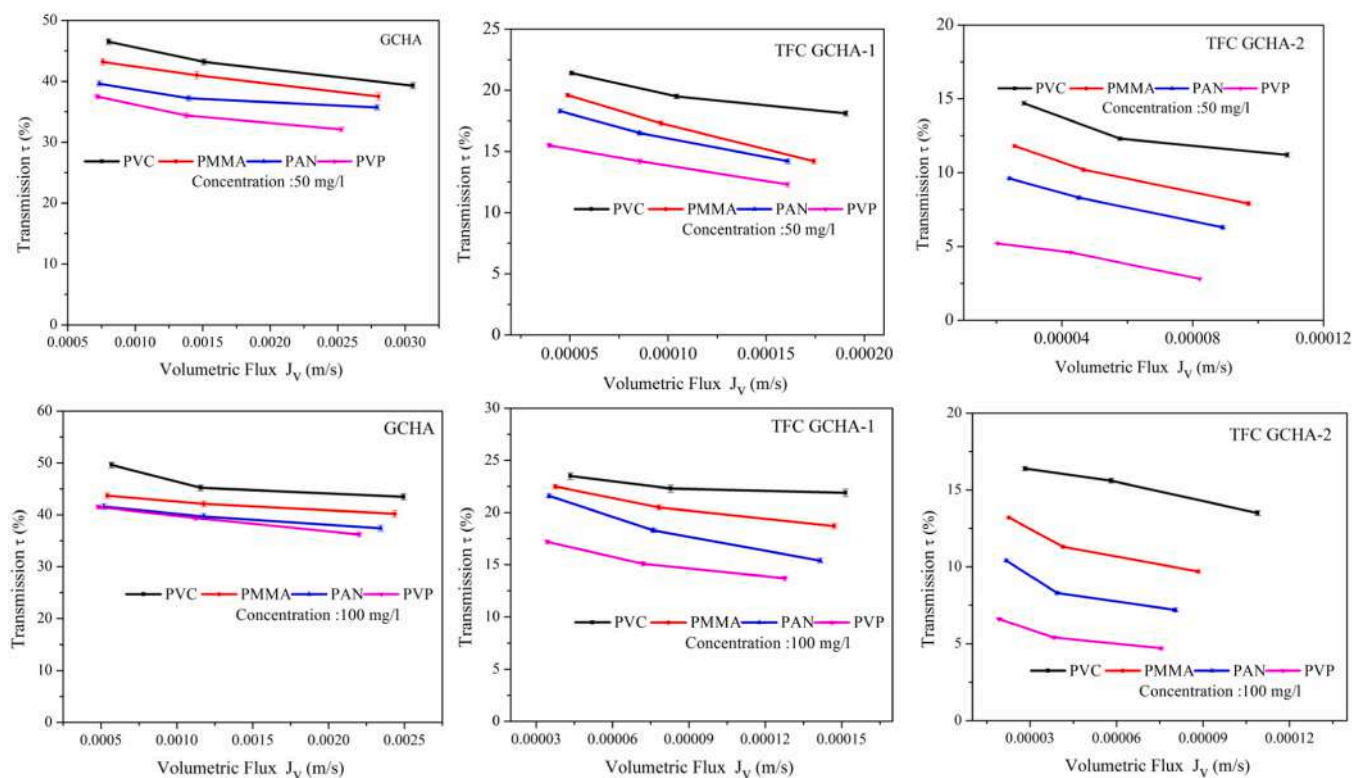


Fig. 6. MPs flux (J_v) and transmission (τ) analysis of GCHA, and TFC-GCHA membranes with respect to different TMP (50, 100 and 200 kPa) and concentration (50 mg/L and 100 mg/L).

volumetric flux reduced in both TFC-GCHA membranes, which was due to the lower pore size. PVP displayed the lowest J_v and transmission as compared to other MPs regardless of the type of membrane used. This observation was attributed to higher molecular weight of PVP (360,000 Da) and PVP solubility enhancing the viscosity of water. TFC-GCHA-2 membrane exhibited the lowest PVP transmission of 2.7 (%) for the concentration of 50 mg/L. This could be due to the existence of a dense selective poly (piperazine-amide) layer in TFC-GCHA-2 membrane. PVC solution held the highest transmission of 49% through GCHA membrane at a TMP of 200 kPa for 100 mg/L. It was important to observe that the increase of MPs concentration from 50 to 100 mg/L increased its concentration in the permeate. The MPs removal efficiency is in the order of PVP > PAN > PMMA > PVC. The physicochemical properties of MPs played a significant role in governing the filtration behavior. The molecular weight of PVC, PMMA and PAN are within the range of 80,000–120,000 Da. All the membranes displayed an increase in volumetric flux when the MPs concentration decreased. Furthermore, the increase of TMP decreased the transmission of MPs. This is due to the fact that high molecular weight MPs initially adsorb and form polarization layer on the membrane surface. Other factors which contributed to the interaction of GCHA and TFC-GCHA membranes include hydrophobicity (vinyl chloride in PVC, methyl methacrylate in PMMA and acrylonitrile in PAN), surface charge (dissociation of MPs in water causes exchange of surface functional groups) and particle sizes (beads: PMMA and amorphous: PVC and PAN) (Zhang et al., 2021b). Both experimental flux and observed transmission data were in good agreement with the concentration polarization model. The similar pattern of protein flux and transmission on ultrafiltration (UF) membrane was noticed in literature (Narsaiah and Agarwal, 2007). As seen in Fig. 5, the transmission (%) of MPs is even lower for 100 mg/L in TFC-GCHA HF-2 membranes. On the basis of MPs removal, the membrane performance is in the order of TFC-GCHA-2 > TFC-GCHA-1 > GCHA membranes. The TFC-GCHA membranes outperformed the GCHA membranes due to the selective polyamide layer which acts as a barrier for the transmission of

MPs. The higher concentration of amine monomer contributed to the formation of interconnected dense pores on the surface of TFC-GCHA-2 membranes which minimized the adsorption of MPs onto the ceramic substrate. This MPs filtration analysis indicated that TFC-GCHA membrane displayed better performance at lower TMP (200 kPa) and concentration (50 mg/L).

3.5.2. Impact of foulants on MPs filtration analysis of GCHA and TFC-GCHA membranes

Natural organic matters (NOM) and extracellular polymeric substances (EPS) are common foulants found in waterways. These macromolecules can easily buildup and block the membrane pores during filtrations (Alresheedi et al., 2019). Fig. 7 shows the effect of HA and SA on MPs filtration at a TMP of 50–200 kPa. GCHA membrane exhibited the highest flux and transmission percentage for both HA-MPs and SA-MPs solutions. All membranes exhibited a drop in flux for the MPs-HA and MPs-SA filtration as compared to the filtration using individual MPs (Fig. 6). GCHA membrane exhibited the highest transmission of 41.5% for 50 mg/L PVC: 50 mg/L SA solution at a TMP of 50 kPa. Lower transmission was observed in both TFC-GCHA membranes for both HA-MPs and SA-MPs solutions. TFC-GCHA-2 membrane displayed the lowest transmission of 4.1% for 50 mg/L PVP: 50 mg/L HA solution at a TMP of 200 kPa. The presence of the polyamide layer has restricted the transport of MPs via sieving mechanism. The filtration analysis was in good agreement with mass transfer coefficient data analysis of MPs. Table 2 shows the MPs mass transfer coefficient data of the membranes and the value of R^2 are also close to one. In concentration polarization phenomena, mass transfer coefficient relies on both flux and transmission of MPs. The solute movement restricted with the enhancement of flux, owing to the accumulation of solute molecule on membrane surface and adsorption or blocking solute molecules on the membrane surface. The mass transfer coefficient factor is an estimation of the solute molecule diffusion from feed to membrane interface (Shamsuddin et al., 2015). For MPs, the desired mass transfer coefficient should be of a

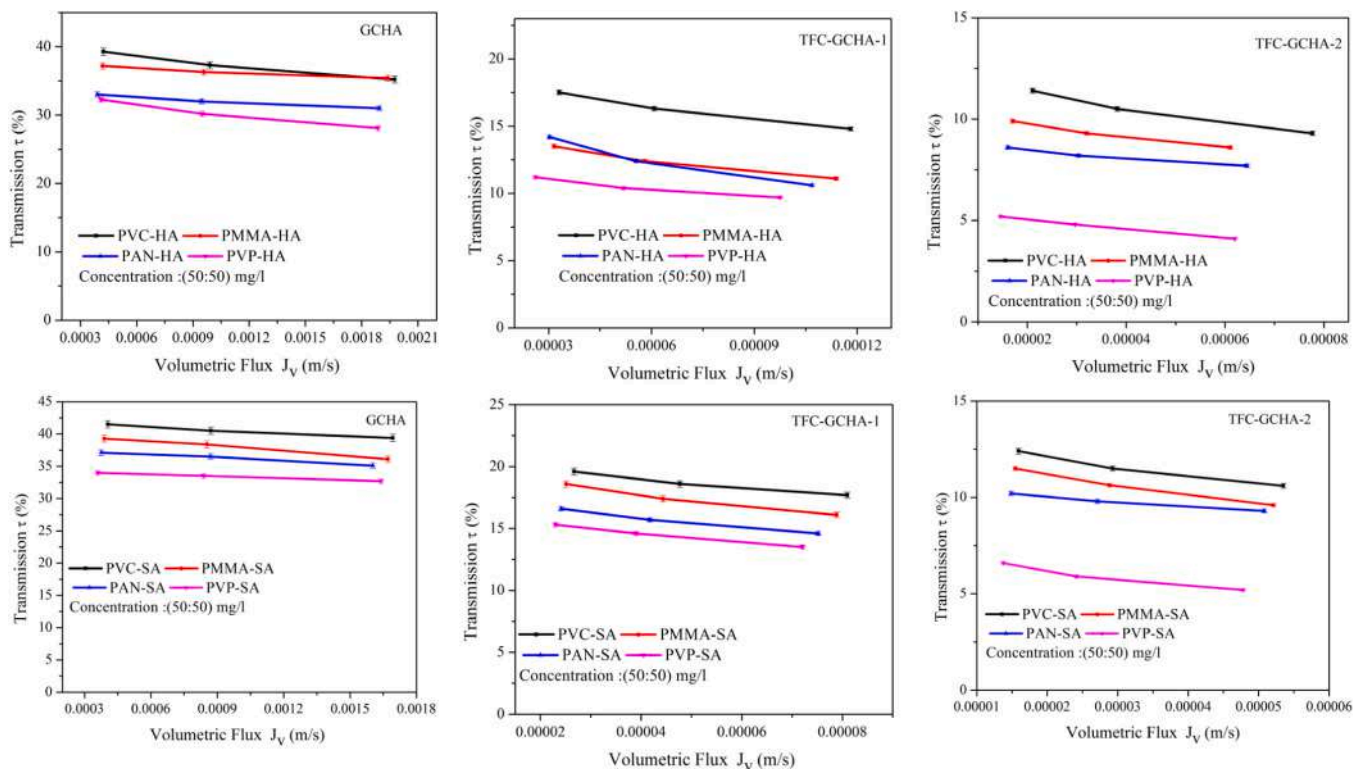


Fig. 7. MPs with organic foulants (humic acid (HA) and sodium alginate (SA)) flux (J_v) and transmission (τ) analysis of GCHA, and TFC-GCHA membranes with respect to different TMP (50, 100 and 200 kPa) and concentration (MP: organic foulants) (50 mg/L:50 mg/L).

Table 2

MPs mass transfer coefficient, FRR and R^2 data of GCHA and TFC-GCHA membranes.

Membrane	GCHA	TFC-GCHA-1	TFC-GCHA-2
PVC-HA			
$k(\text{ms}^{-1})$	0.0090	0.00044	0.00021
R^2	0.979	0.987	0.997
(%)FRR	13.73	6.01	0.97
PMMA-HA			
$k(\text{ms}^{-1})$	0.022	0.00037	0.00029
R^2	0.980	0.991	0.986
(%)FRR	16.60	9.78	5.73
PAN-HA			
$k(\text{ms}^{-1})$	0.0167	0.00024	0.00042
R^2	0.974	0.976	0.977
(%)FRR	20.49	11.71	6.17
PVP-HA			
$k(\text{ms}^{-1})$	0.0076	0.00046	0.00019
R^2	0.982	0.967	0.999
(%)FRR	26.66	14.80	7.27
PVC-SA			
$k(\text{ms}^{-1})$	0.0151	0.00044	0.00021
R^2	0.984	0.978	0.982
(%)FRR	15.26	7.74	3.51
PMMA-SA			
$k(\text{ms}^{-1})$	0.0093	0.00031	0.00019
R^2	0.991	0.985	0.991
(%)FRR	17.06	12.92	5.70
PAN-SA			
$k(\text{ms}^{-1})$	0.014	0.00034	0.00036
R^2	0.993	0.989	0.989
(%)FRR	22.33	11.71	7.55
PVP-SA			
$k(\text{ms}^{-1})$	0.022	0.00034	0.00014
R^2	0.999	0.996	0.964
(%)FRR	28.30	14.27	10.65

lower value. GCHA membrane displayed the highest mass transfer

coefficient for in all the MPs in which maximum of 0.022 ms^{-1} for PMMA-HA and PVP-SA was observed. The proximity of MPs mass transfer coefficient value was due to flux and transmission data are closer to another. The complex formation of organic foulant with MPs is also other reason. From Table 2, mass transfer coefficient value decreased imperatively for TFC-GCHA membranes, which also revealed that MP and foulant transmission (τ) was lower. Lowest mass transfer coefficient of 0.00014 ms^{-1} was noticed in TFC-GCHA-2 membrane for PVP-SA. The lower mass transfer coefficient in TFC-GCHA membrane could be due to two main reasons (i) solubility properties of MPs and NOM and (ii) membrane surface. As seen in Fig. 7, the transmission (τ) % of PVP based HA and SA solutions were lower in both GCHA and TFC-GCHA membranes. This phenomenon was due to the solubility of PVP enhances interaction with HA and SA and ultimately result in complex formation. The other MPs are belongs to suspended type and hydrophobic characteristics. Fig. 8a shows the FTIR spectra of MPs. Hydrophobic alkane (C-H) stretching peak is seen at the wavelength range of $2908\text{--}2993 \text{ cm}^{-1}$ in all the MPs (Kuang et al., 2019; Ramesh et al., 2007; Safo et al., 2019). The other prominent hydrophobic groups such as CH_3 , C-Cl stretching were noticed in PMMA and PVC, respectively (Ramesh et al., 2007). The C-N stretching belongs to the pyrrolidone and nitrile group are clearly seen in PVP and PAN, respectively (Kuang et al., 2019; Safo et al., 2019). The hydrophilic carboxylic group was distinctly visible in PVP. The possible interaction of MPs and foulant is shown in Fig. 8b. Upon filtration, the larger MPs-HA and MPs-SA complexes are bound to the membrane surface and block water transport. The MPs fouling analysis exhibited good correlation with the physiochemical properties of MPs solution.

The FRR data of membranes for MPs-HA and MPs-SA are shown in Table 2. GCHA membrane displayed the highest FRR for the MPs-HA and MPs-SA solutions. GCHA membrane exhibited FRR of 28.30% for the PVP-SA solution. It indicated that the MPs adsorbed on the surface and pore walls of membrane, due to larger pore size and higher surface roughness of the membrane (Fig. 3). The FRR values were significantly

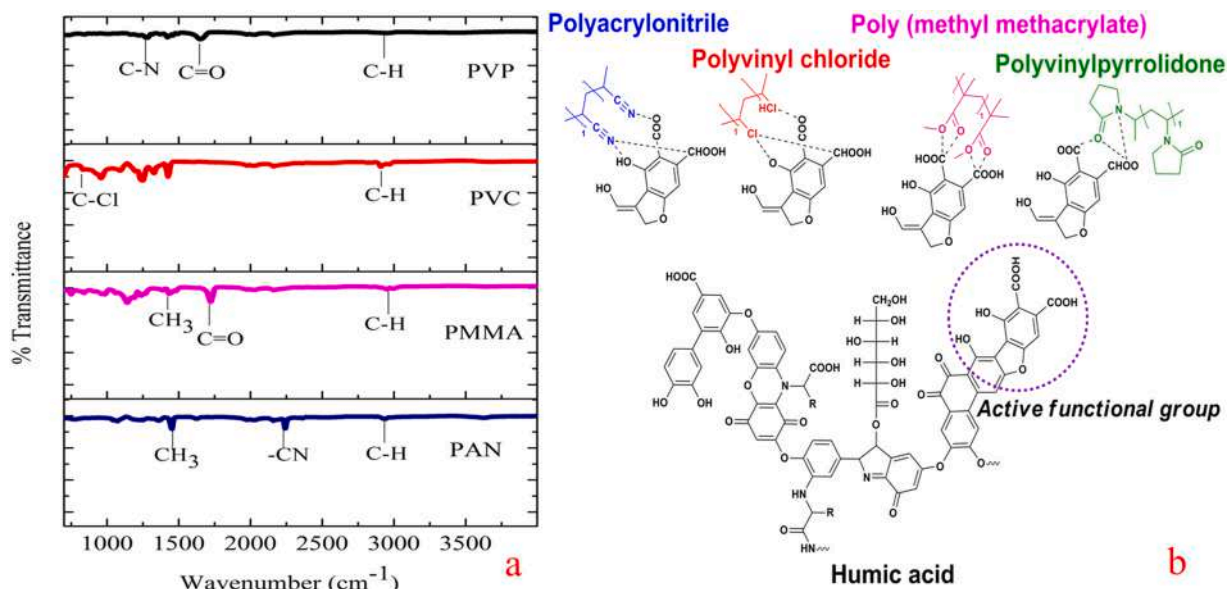


Fig. 8. MPs Functional group analysis. 8a. FTIR spectra of MP, 8b. Schematic of MPs-HA interactions.

reduced in both TFC-GCHA membranes. TFC-GCHA-2 membrane exhibited lower FRR of 0.97% for PVC-HA solution. This could be due to the reduced pore size and surface area on the membrane substructures for the attachment of MPs. Schematic illustration of MP fouling is presented in Fig. 9a. MPs-HA solution displayed slightly lower FRR compared to MPs-SA. It is due to the MPs bind strongly with active sites of HA through anionic interactions, particularly from the carboxylic group. HA also constitutes enormous active sites of hydroxyl ions, which tend to binds with heteroatoms of MPs (-N- in PAN, -Cl- in PVC, -COO⁻ in PMMA, and -N- as well as -COO⁻ in PVP). Thus, lower transmission and FRR was observed for MPs-HA as compared to MPs-SA. However, the interaction between MPs and SA was weaker, due to the masking of Na⁺ ions in SA active functional sites. MPs-SA exhibited lower flux and higher transmission for both GCHA and TFC-GCHA membranes (Fig. 7). This could be due to the binding of SA on the membrane surface which has restricted the water movement. Membrane functional group analysis was also studied to evaluate the interaction between feed and membrane. Fig. 9b shows the FTIR spectra of GCHA and TFC-GCHA-2

membranes before and after filtration. The characteristic spectral band of Si-O-Si vibration was observed at 1012.08 cm^{-1} for both membranes and another Si stretch was also observed at 789.71 cm^{-1} (Wang et al., 2020a, 2020b, 2020c). As seen in Fig. 9b, the intensity of both GCHA and TFC-GCHA-2 membranes remained the same and no foulant peaks were noticed. This confirms that foulant deposition was minimal on both membranes, which could be due to the lower concentration of MPs (50 mg/L) and foulants (50 mg/L). Overall, the MPs filtration indicated that the TFC-GCHA-2 exhibited lower MPs transmission which makes it an ideal membrane for the separation of MPs from aqueous solution.

3.6. Impact of TFC-GCHA membranes on seawater pretreatment

Primary (cosmetics) and secondary MPs (degradation of macroplastic) are the main source of marine pollutants, which enter into seawater through surface water, industrial effluents, atmospheric contaminants and trash materials (Jiang et al., 2022). Fig. 10a shows the cycles of pretreatment of untreated seawater filtration analysis of TFC

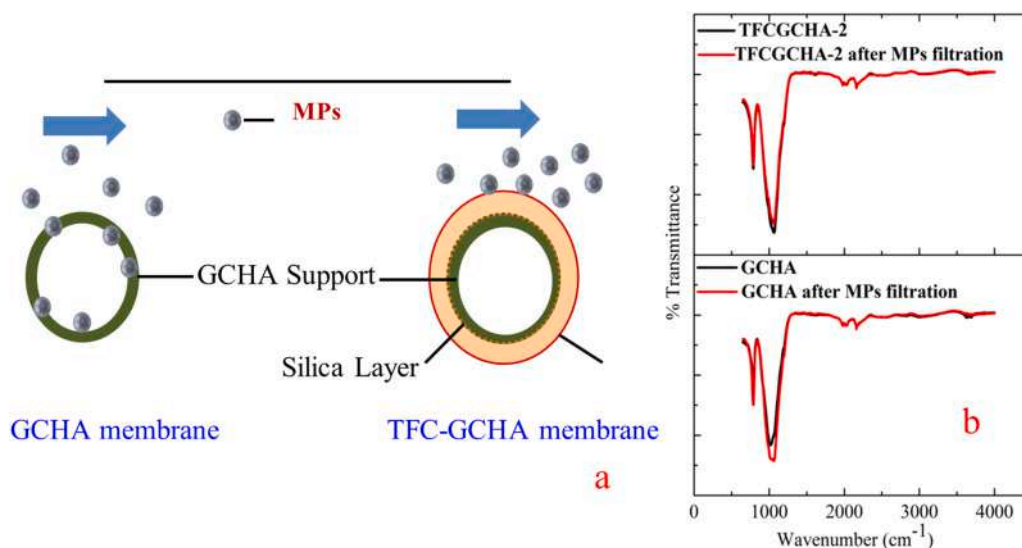


Fig. 9. MPs fouling analysis. 9a. Schematic of MPs fouling in GCHA and TFC-GCHA membranes. 9b. FTIR spectra of before and after MPs analysis of GCHA and TFC-GCHA membranes.

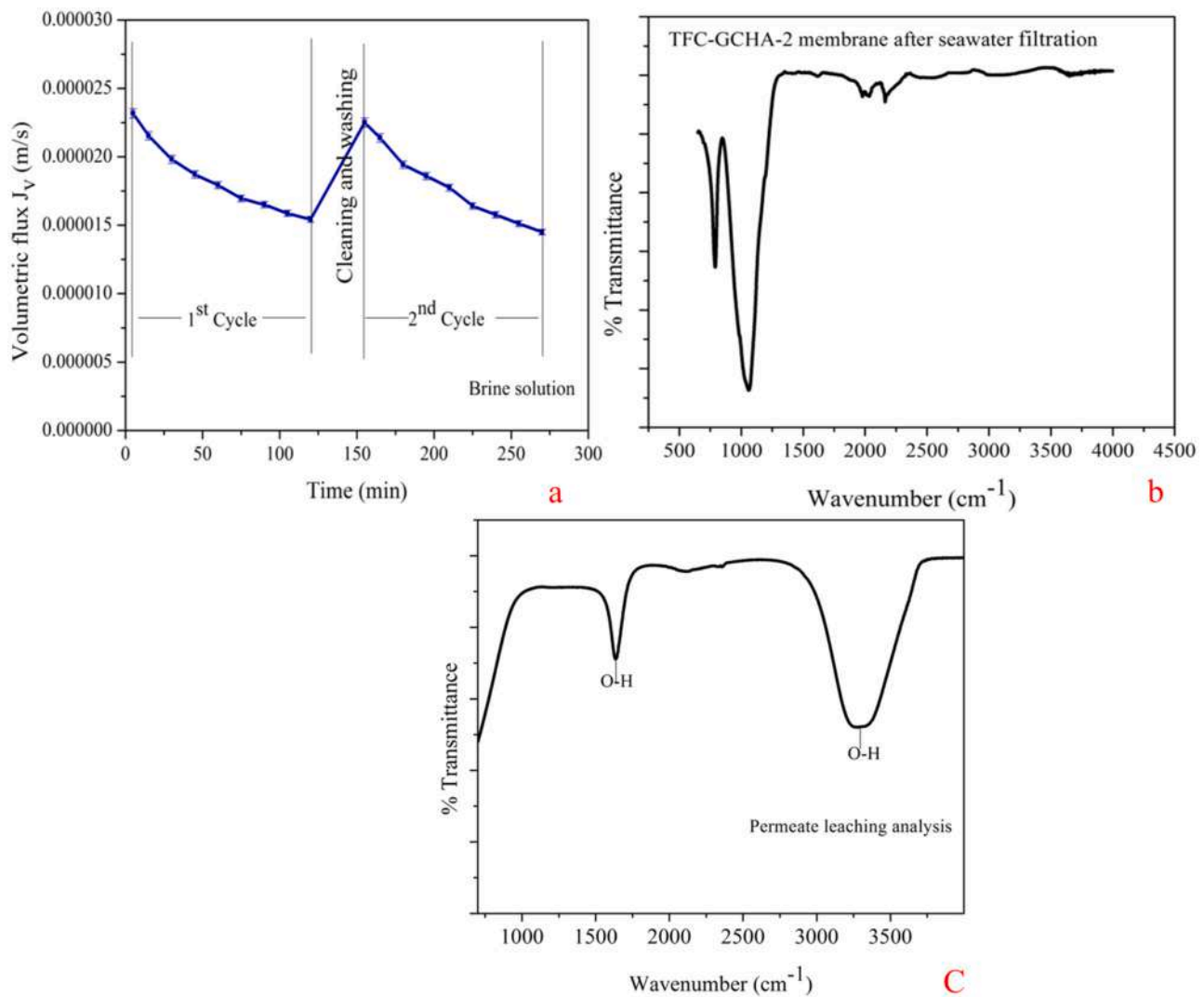


Fig. 10. Brine solution filtration analysis of TFC-GCHA-2 membranes. 10a. Flux analysis with respect to time, 10b. FTIR analysis of membrane after brine water filtration. 10c. Permeate leaching analysis.

GCHA-2 HF membrane at a TMP of 100 kPa. As seen in Fig. 10a, the flux decreased with the increase of seawater filtration duration. This could be due to (i) adsorption of colloidal particles in seawater on poly (piperazine-amide) layer and (ii) blocking of smaller inorganic substances on interior pore walls of membrane pores. Such accumulation minimized the movement of water molecules through the polymeric and ceramic matrix. An average steady state flux and ionic transmission of

0.19×10^{-4} m/s and 100% was noticed with the low TMP of 100 kPa. The higher selectivity was due to the large membranes pore size. It was imperative to mention that the flux values were consistent for both cycles and FRR was less than 27% for TFC-GCHA-2 HF membranes. This indicated that the formation of poly (piperazine-amide) layer restricted the attachment of foulants on the surface of membrane, mitigating fouling. Fig. 10b shows the FTIR analysis of TFC GCHA-2 membrane

Table 3
Performance evaluation of MPs filtration with literatures.

S. No	Membrane	MPs	Rejection (%)	Flux ($\times 10^{-4}$ m/s)	Transport mechanism	References
1	PEI and PAA modified electrospun polyacrylonitrile	polystyrene	99	2.39	sieving and electrostatic attraction	(Wang et al., 2020b)
2	Poly(sulfone)	poly(ethylene)	80–50	$\sim 0.21^{**}$	cake layer	(Enfrin et al., 2020)
3	Cellulose acetate	polyamide	99.8	96.7*	sieving	(Pizzichetti et al., 2021)
5	TFC-GCHA-2	polystyrene	94.3			
		PVC (50 mg/L)	88.8	1.09	concentration polarization	Present study
		PMMA (50 mg/L)	92.1	0.97		
		PAN (50 mg/L)	93.7	0.89		
		PVP (50 mg/L)	97.2	0.82		
		Seawater	100% ionic transmission	0.19		

** - Steady state flux under longer duration.

* - After 10 min of filtration.

after seawater filtration. The membrane surface functional group was unchanged even after filtration. This further confirmed that the TFC GCHA-2 membrane was resilient and exhibited great potential for real time water reclamation applications. Table 3 shows the MPs filtration performance comparison of membrane prepared in this work with membranes found in literature. Among the membranes, silica GCHA based TFC membrane displayed better and comparable MPs removal performance and selectivity for seawater filtration. TFC GCHA-2 membrane also displayed fouling resistant for seawater and comparable flux under energy efficient condition of low TMP. The leaching test of membrane was also assessed after seawater filtration using municipal water. As seen in Fig. 10 c, the FTIR peak showed only hydroxyl peaks. It revealed that no residues of MPs or other constituents from membrane in the permeate. The superior stability of membrane was due to the strong bonding of thin poly (piperazine-amide) layer on GCHA support through intermediate silica layer via interfacial polymerization and electrostatic attraction. This can ascribed to the presence of electron rich silica, which has strong affinity to bind with amine group in piperazine. The intermediate silica layer provided roughness and hydrophilicity for the controlled diffusion of monomers and aid in resilient thin film formation. Similar interlayer structures also improved the stability of ceramic membranes (Cho et al., 2021; Li et al., 2021). In general, high pressure reverse osmosis (RO) membranes are widely deployed for the production of potable water from brackish water. The existence of MPs cause membrane fouling and decline the performance of membrane. This study provides an insight on an effective modification and ecofriendly method in preparing a highly porous ceramic membrane for the pre-treatment of MPs prior to seawater RO desalination. Thereby, GCHA based TFC membrane can ensure a sustainable production of freshwater.

4. Conclusion

Cost effective GCHA supported TFC membranes were successfully fabricated via interfacial polymerization and tested for their MP removal efficiency in aqueous solution. Cross sectional analysis confirmed the formation of polyamide layer over asymmetric GCHA HF membrane. AFM analysis indicated that a regular pore structures were noticed in TFC-GCHA membranes with lower surface area for membrane prepared with higher monomer concentration. Water flux analysis elucidated that TFC-GCHA-2 membrane exhibited lower water flux of 296.58 L/m²h, owing to the formation of a thin polyamide layer. The smaller polyamide layer pore was clearly seen during MIP analysis. During MPs filtration, TFC-GCHA membranes exhibited lower transmission for all MPs solutions. Volumetric flux increased with the increase of TMP and decreased MPs transmission. The flux and transmission data had good correlation with concentration polarization model. The organic foulant HA and SA inhibited the flux for all membranes. MP-HA increased the transmission in all the membranes, owed to complex formation. Flux dropped and transmission increased in the presence of MPs-SA. TFC-GCHA membranes displayed lower MPs transmission of MPs for all foulants. TFC-GCHA-2 membrane exhibited lower FRR with better stability during the long-term seawater filtration. Overall, this study reveals the potential of GCHA supported HF TFC membranes as an energy efficient and economic material for MPs filtration.

CRedit authorship contribution statement

Lukka Thuyavan Yogarathinam: Conceptualization, Investigation, Writing - original draft, **Jamilu Usman:** Conceptualization & Methodology, **Mohd Hafiz Dzarfan Othman:** Writing - review & editing, Resources, **Ahmad Fauzi Ismail:** Supervision, Project administration, Resources, **Pei Sean Goh:** Writing - review & editing, Visualization, **Arthanareeswaran Gangasalam:** Writing - review & editing, **Mohd Ridhwan Adam:** Investigation & Methodology.

Declaration of Competing Interest

The authors declare that they have no known competing financial interests or personal relationships that could have appeared to influence the work reported in this paper.

Acknowledgements

The authors would like to thank the Higher Institution Centre of Excellence (HiCOE) Advanced Membrane Technology Research Centre (AMTEC), Universiti Teknologi Malaysia (UTM) and Research Management Centre (RMC) for the support and encouragement (UTM J.13.01/13.14/1/88.Jld. 19(17)).

References

- Adam, M.R., Matsuura, T., Othman, M.H.D., Puteh, M.H., Pauzan, M.A.B., Ismail, A.F., Mustafa, A., Rahman, A., Jaafar, M., Abdullah, M.S., 2019. Feasibility study of the hybrid adsorptive hollow fibre ceramic membrane (HFCM) derived from natural zeolite for the removal of ammonia in wastewater. *Process Saf. Environ. Prot.* 122, 378–385. <https://doi.org/10.1016/j.psep.2018.12.003>.
- Alftessi, S.A., Othman, M.H.D., Adam, M.R., Farag, T.M., Ismail, A.F., Rahman, M.A., Jaafar, J., Habib, M.A., Raji, Y.O., Hubadillah, S.K., 2021. Novel silica sand hollow fibre ceramic membrane for oily wastewater treatment. *J. Environ. Chem. Eng.* 9, 104975 <https://doi.org/10.1016/j.jece.2020.104975>.
- Alresheedi, M.T., Barbeau, B., Basu, O.D., 2019. Comparisons of NOM fouling and cleaning of ceramic and polymeric membranes during water treatment. *Sep. Purif. Technol.* 209, 452–460. <https://doi.org/10.1016/j.seppur.2018.07.070>.
- Bello, M.O., Abdus-Salam, N., Adekola, F.A., 2018. Utilization of guinea corn (Sorghum vulgare) husk for preparation of bio-based silica and its characterization studies. *Int. J. Environ. Agric. Biotechnol.* 3, 670–675. <https://doi.org/10.22161/ijeab/3.2.48>.
- Bilal, M., Iqbal, H.M.N., 2020. Transportation fate and removal of microplastic pollution – a perspective on environmental pollution. *Case Stud. Chem. Environ. Eng.* 2, 100015 <https://doi.org/10.1016/j.csee.2020.100015>.
- Chong, J.Y., Wang, R., 2019. From micro to nano: polyamide thin film on microfiltration ceramic tubular membranes for nanofiltration. *J. Membr. Sci.* 587 <https://doi.org/10.1016/j.memsci.2019.06.001>.
- Cho, Y.H., Jeong, S., Kim, S.J., Kim, Y., Lee, H.J., Lee, T.H., Park, H.B., Park, H., Nam, S. E., Park, Y.I., 2021. Sacrificial graphene oxide interlayer for highly permeable ceramic thin film composite membranes. *J. Membr. Sci.* 618, 118442 <https://doi.org/10.1016/j.memsci.2020.118442>.
- Dick Vethaak, A., Legler, J., 2021. Microplastics and human health: Knowledge gaps should be addressed to ascertain the health risks of microplastics. *Science* 371 (80), 672–674. <https://doi.org/10.1126/science.abe5041>.
- Enfrin, M., Lee, J., Fane, A.G., Dumée, L.F., 2021. Mitigation of membrane particulate fouling by nano / microplastics via physical cleaning strategies. *Sci. Total Environ.* 788, 147689 <https://doi.org/10.1016/j.scitotenv.2021.147689>.
- Enfrin, M., Lee, J., Le-Clech, P., Dumée, L.F., 2020. Kinetic and mechanistic aspects of ultrafiltration membrane fouling by nano- and microplastics. *J. Membr. Sci.* 601 <https://doi.org/10.1016/j.memsci.2020.117890>.
- Fard, A.K., McKay, G., Buekenhoudt, A., Al Sulaiti, H., Motmans, F., Khraisheh, M., Ateih, M., 2018. Inorganic membranes: preparation and application for water treatment and desalination. In: *Materials (Basel)*, 11. <https://doi.org/10.3390/ma11010074>.
- Gohil, J.M., Ray, P., 2017. A review on semi-aromatic polyamide TFC membranes prepared by interfacial polymerization: potential for water treatment and desalination. *Sep. Purif. Technol.* 181, 159–182. <https://doi.org/10.1016/j.seppur.2017.03.020>.
- Hubadillah, S.K., Othman, M.H.D., Harun, Z., Ismail, A.F., Rahman, M.A., Jaafar, J., Jamil, S.M., Mohtar, N.H., 2017. Superhydrophilic, low cost kaolin-based hollow fibre membranes for efficient oily-wastewater separation. *Mater. Lett.* 191, 119–122. <https://doi.org/10.1016/j.matlet.2016.12.099>.
- Hubadillah, S.K., Othman, M.H.D., Matsuura, T., Rahman, M.A., Jaafar, J., Ismail, A.F., Amin, S.Z.M., 2018. Green silica-based ceramic hollow fiber membrane for seawater desalination via direct contact membrane distillation. *Sep. Purif. Technol.* 205, 22–31. <https://doi.org/10.1016/j.seppur.2018.04.089>.
- Hubadillah, S.K., Othman, M.H.D., Tai, Z.S., Jamalludin, M.R., Yusuf, N.K., Ahmad, A., Rahman, M.A., Jaafar, J., Kadir, S.H.S.A., Harun, Z., 2020. Novel hydroxyapatite-based bio-ceramic hollow fiber membrane derived from waste cow bone for textile wastewater treatment. *Chem. Eng. J.* 379, 122396 <https://doi.org/10.1016/j.cej.2019.122396>.
- Jamalludin, M.R., Hubadillah, S.K., Harun, Z., Othman, M.H.D., Yunus, M.Z., 2019. Novel superhydrophobic and superoleophilic sugarcane green ceramic hollow fiber membrane as hybrid oil sorbent-separator of real oil and water mixture. *Mater. Lett.* 240, 136–139. <https://doi.org/10.1016/j.matlet.2018.12.111>.
- Jiang, Y., Yang, F., Hassan Kazmi, S.S.U., Zhao, Y., Chen, M., Wang, J., 2022. A review of microplastic pollution in seawater, sediments and organisms of the Chinese coastal and marginal seas. *Chemosphere* 286, 131677. <https://doi.org/10.1016/j.chemosphere.2021.131677>.

- Khanmohammadi, S., Taheri-Nassaj, E., Farrokhi-Rad, M., 2020. Synthesis of mesoporous gamma-alumina membrane: effect of yttria addition on the thermal stability. *Surf. Interfaces* 21, 100683. <https://doi.org/10.1016/j.surfin.2020.100683>.
- Khorshidi, B., Thundat, T., Fleck, B.A., Sadrzadeh, M., 2015. Thin film composite polyamide membranes: parametric study on the influence of synthesis conditions. *RSC Adv.* 5, 54985–54997. <https://doi.org/10.1039/c5ra08317f>.
- Kuang, Y., He, H., Chen, S., Wu, J., Liu, F., 2019. Adsorption behavior of CO₂ on amine-functionalized polyacrylonitrile fiber. *Adsorption* 25, 693–701. <https://doi.org/10.1007/s10450-019-00070-0>.
- Kumar, M., Chen, H., Sarsaiya, S., Qin, S., Liu, H., Awasthi, M.K., Kumar, S., Singh, L., Zhang, Z., Bolan, N.S., Pandey, A., Varjani, S., Taherzadeh, M.J., 2021a. Current research trends on micro- and nano-plastics as an emerging threat to global environment: a review. *J. Hazard. Mater.* 409, 124967 <https://doi.org/10.1016/j.jhazmat.2020.124967>.
- Kumar, R., Sharma, P., Manna, C., Jain, M., 2021b. Abundance, interaction, ingestion, ecological concerns, and mitigation policies of microplastic pollution in riverine ecosystem: a review. *Sci. Total Environ.* 782, 146695 <https://doi.org/10.1016/j.scitotenv.2021.146695>.
- Li, P., Li, Y.X., Wu, Y.Z., Xu, Z.L., Zhang, H.Z., Gao, P., Xu, S.J., 2021. Thin-film nanocomposite NF membrane with GO on macroporous hollow fiber ceramic substrate for efficient heavy metals removal. *Environ. Res.* 197, 111040 <https://doi.org/10.1016/j.envres.2021.111040>.
- Lohokare, H.R., Muthu, M.R., Agarwal, G.P., Kharul, U.K., 2008. Effective arsenic removal using polyacrylonitrile-based ultrafiltration (UF) membrane. *J. Membr. Sci.* 320, 159–166. <https://doi.org/10.1016/j.memsci.2008.03.068>.
- Lukka Thuyavan, Y., Arthanareeswaran, G., Ismail, A.F., Goh, P.S., Shankar, M.V., Ng, B. C., Sathish Kumar, R., Venkatesh, K., 2021. Binary metal oxides incorporated polyethersulfone ultrafiltration mixed matrix membranes for the pretreatment of seawater desalination. *J. Appl. Polym. Sci.*, e49883 <https://doi.org/10.1002/app.49883>.
- Narsaiah, K., Agarwal, G.P., 2007. Transmission analysis in ultrafiltration of ternary protein mixture through a hydrophilic membrane. *J. Membr. Sci.* 287, 9–18. <https://doi.org/10.1016/j.memsci.2006.10.001>.
- Ouaddari, H., Karim, A., Achiou, B., Saja, S., Aaddane, A., Bennazha, J., El Amrani El Hassani, L., Ouammou, M., Albizane, A., 2019. New low-cost ultrafiltration membrane made from purified natural clays for direct Red 80 dye removal. *J. Environ. Chem. Eng.* 7, 103268 <https://doi.org/10.1016/j.jece.2019.103268>.
- Pizzichetti, A.R.P., Pablos, C., Álvarez-Fernández, C., Reynolds, K., Stanley, S., Marugán, J., 2021. Evaluation of membranes performance for microplastic removal in a simple and low-cost filtration system. *Case Stud. Chem. Environ. Eng.* 3, 100075 <https://doi.org/10.1016/j.csee.2020.100075>.
- Ramesh, S., Leen, K.H., Kumutha, K., Arof, A.K., 2007. FTIR studies of PVC/PMMA blend based polymer electrolytes. *Spectrochim. Acta - Part A Mol. Biomol. Spectrosc.* 66, 1237–1242. <https://doi.org/10.1016/j.saa.2006.06.012>.
- Safo, I.A., Werheid, M., Dosche, C., Oezaslan, M., 2019. The role of polyvinylpyrrolidone (PVP) as a capping and structure-directing agent in the formation of Pt nanocubes. *Nanoscale Adv.* 1, 3095–3106. <https://doi.org/10.1039/c9na00186g>.
- Seah, M.Q., Lau, W.J., Goh, P.S., Tseng, H.H., Wahab, R.A., Ismail, A.F., 2020. Progress of interfacial polymerization techniques for polyamide thin film (Nano)composite membrane fabrication: a comprehensive review. *Polymers* 12, 2817. <https://doi.org/10.3390/polym12122817>.
- Shamsuddin, N., Das, D.B., Starov, V.M., 2015. Filtration of natural organic matter using ultrafiltration membranes for drinking water purposes: circular cross-flow compared with stirred dead end flow. *Chem. Eng. J.* 276, 331–339. <https://doi.org/10.1016/j.cej.2015.04.075>.
- Sun, J., Dai, X., Wang, Q., van Loosdrecht, M.C.M., Ni, B.J., 2019. Microplastics in wastewater treatment plants: detection, occurrence and removal. *Water Res.* 152, 21–37. <https://doi.org/10.1016/j.watres.2018.12.050>.
- Usman, J., Othman, M.H.D., Ismail, A.F., Rahman, M.A., Jaafar, J., Raji, Y.O., El Badawy, T.H., Gbadamosi, A.O., Kurniawan, T.A., 2020. Impact of organosilanes modified superhydrophobic-superoleophilic kaolin ceramic membrane on efficiency of oil recovery from produced water. *J. Chem. Technol. Biotechnol.* 95, 3300–3315. <https://doi.org/10.1002/jctb.6554>.
- Van Gestel, T., Kruidhof, H., Blank, D.H.A., Bouwmeester, H.J.M., 2006. ZrO₂ and TiO₂ membranes for nanofiltration and pervaporation. Part 1. Preparation and characterization of a corrosion-resistant ZrO₂ nanofiltration membrane with a MWCO < 300. *J. Membr. Sci.* 284, 128–136. <https://doi.org/10.1016/j.memsci.2006.07.020>.
- Vinoth Kumar, R., Kumar Ghoshal, A., Pugazhenthii, G., 2015. Elaboration of novel tubular ceramic membrane from inexpensive raw materials by extrusion method and its performance in microfiltration of synthetic oily wastewater treatment. *J. Membr. Sci.* 490, 92–102. <https://doi.org/10.1016/j.memsci.2015.04.066>.
- Wang, W., Ge, J., Yu, X., Li, H., 2020a. Environmental fate and impacts of microplastics in soil ecosystems: progress and perspective. *Sci. Total Environ.* 708, 134841 <https://doi.org/10.1016/j.scitotenv.2019.134841>.
- Wang, Z., Hao, L., Yang, F., Wei, Q., 2020b. Mesoporous silica membranes silylated by fluorinated and non-fluorinated alkylsilanes for the separation of methyl tert-butyl ether from water. *Membranes* 10 (4), 70. <https://doi.org/10.3390/membranes10040070>.
- Wang, R., Zhang, L., Chen, B., Zhu, X., 2020c. Low-pressure driven electrospun membrane with tuned surface charge for efficient removal of polystyrene nanoplastics from water. *J. Membr. Sci.* 614, 118470 <https://doi.org/10.1016/j.memsci.2020.118470>.
- Wei, J., Liu, X., Qiu, C., Wang, R., Tang, C.Y., 2011. Influence of monomer concentrations on the performance of polyamide-based thin film composite forward osmosis membranes. *J. Membr. Sci.* 381, 110–117. <https://doi.org/10.1016/j.memsci.2011.07.034>.
- Xia, L., Ren, J., Weyd, M., McCutcheon, J.R., 2018. Ceramic-supported thin film composite membrane for organic solvent nanofiltration. *J. Membr. Sci.* 563, 857–863. <https://doi.org/10.1016/j.memsci.2018.05.069>.
- Yan, H., Miao, X., Xu, J., Pan, G., Zhang, Y., Shi, Y., Guo, M., Liu, Y., 2015. The porous structure of the fully-aromatic polyamide film in reverse osmosis membranes. *J. Membr. Sci.* 475, 504–510. <https://doi.org/10.1016/j.memsci.2014.10.052>.
- Yu, L., Kanezashi, M., Nagasawa, H., Tsuru, T., 2020. Phase inversion/sintering-induced porous ceramic microsheet membranes for high-quality separation of oily wastewater. *J. Membr. Sci.* 595, 117477 <https://doi.org/10.1016/j.memsci.2019.117477>.
- Zhang, X., Liu, Z.P., Xu, Z.L., Cheng, F.Y., Ma, X.H., Xu, X.R., 2021a. Thin-film composite membranes fabricated directly on a large-porous ceramic support using poly (4-styrenesulfonic acid) as a scaffold for ethanol dehydration. *J. Membr. Sci.* 619, 118775 <https://doi.org/10.1016/j.memsci.2020.118775>.
- Zhang, M., Yang, J., Kang, Z., Wu, X., Tang, L., Qiang, Z., Zhang, D., Pan, X., 2021b. Removal of micron-scale microplastic particles from different waters with efficient tool of surface-functionalized microbubbles. *J. Hazard. Mater.* 404, 124095 <https://doi.org/10.1016/j.jhazmat.2020.124095>.
- Zhong, Z., Li, D., Zhang, B., Xing, W., 2012. Membrane surface roughness characterization and its influence on ultrafine particle adhesion. *Sep. Purif. Technol.* 90, 140–146. <https://doi.org/10.1016/j.seppur.2011.09.016>.
- Zou, D., Fan, W., Xu, J., Drioli, E., Chen, X., Qiu, M., Fan, Y., 2021. One-step engineering of low-cost kaolin/fly ash ceramic membranes for efficient separation of oil-water emulsions. *J. Membr. Sci.* 621, 118954 <https://doi.org/10.1016/j.memsci.2020.118954>.